Title

Downscaling transpiration rate from field to tree scale

Authors

Couvreur, V
Kandelous, MM
Sanden, BL
et al.

Publication Date

2016-05-01

DOI

10.1016/j.agrformet.2016.02.008

Peer reviewed

Agricultural and Forest Meteorology 221 (2016) 71–77

Contents lists available at ScienceDirect

Agricultural and Forest Meteorology

journal homepage: www.elsevier.com/locate/agrformet

Downscaling transpiration rate from field to tree scale

V. Couvreur[a,*], M.M. Kandelous[a], B.L. Sanden[b], B.D. Lampinen[c], J.W. Hopmans[a]

[a] Department of Land, Air and Water Resources, University of California, 1 Shields Ave., Davis, CA 95616, USA
[b] University of California Cooperative Extension, 1031 S. Mt. Vernon Ave., Bakersfield, CA 93307, USA
[c] Department of Plant Sciences, University of California, 1 Shields Ave., Davis, CA 95616, USA

ARTICLE INFO

Article history:
Received 24 September 2015
Received in revised form 1 February 2016
Accepted 7 February 2016

Keywords:
Downscaling
Tree transpiration
Stem water potential
Soil water storage
Canopy cover
Neural network

ABSTRACT

Estimation of field spatial variability of tree actual evapotranspiration (ET_a) in orchards is key when quantifying water and associated nutrient leaching at the field scale. Though ET_a is often measured at the field scale, spatial variations between individual trees are likely due to local differences in soil water availability and canopy cover. It is therefore that we propose seeking a statistical relation between field ET_a, tree midday stem water potential (MSWP), soil water storage (WS), and tree potential evapotranspiration (ET_c) with relative tree canopy cover (C_{rel}). Four years of soil and almond trees water status data were used to optimize an artificial neural network (ANN), to predict field scale ET_a first, followed by downscaling to the individual tree scale. ANN's using two hidden neurons (11 parameters) proved to be the most accurate (RMSE = 0.0246 mm/h, R^2 = 0.944), seemingly because adding more neurons generated overfitting of noise in the training dataset. C_{rel} was the main source of variability of ET_a, while MSWP was the controlling factor for the tree-scale relative ET. At a given soil WS, almond trees of the drip-irrigated block were less affected by root zone water stress than the fanjet micro-sprinklers block, likely because of soil textural differences between the two main experimental blocks. In wet conditions, the predicted tree ET_a followed a normal distribution (with relative standard deviation of about 5%), which was close to the C_{rel} distribution. However, standard deviation values increased (7.6% for the whole orchard) during periods of water stress.

1. Introduction

Both the occurrence and magnitude of droughts is projected to increase in many regions of the world (Parry et al., 2007; IPCC, 2012), thereby affecting irrigation water availability for the very regions that depend largely on irrigated agriculture (Fischer et al., 2000). Therefore, research improving irrigation efficiency has become key (Stanhill, 1986), for example by fine-tuning of irrigation water application (Kandelous et al., 2012; Couto et al., 2013) and irrigation control systems (Shackel, 2011; Dabach et al., 2013, 2015; Shi et al., 2015) based on crop water needs. Central to the effectiveness of improved irrigation management systems is the control of leaching rates. However, the latter has proven difficult to quantify due to difficulties in monitoring leaching confounded by large field-scale variations due to irrigation water applications and soil heterogeneities. Leaching is typically computed from the field water balance method (Tanji and Kielen, 2002) or by inverse modeling (Eching et al., 1994; Hopmans and Schoups, 2005). However, both methods rely on accurate estimations of the crop's actual evapotranspiration rate (ET_a), which typically varies widely across a farmer's field.

For orchards, a common method to estimate tree scale transpiration rate involve sap flow measurements using heat pulse probes. Such sap flow measurements provide a qualitative proxy of tree transpiration rate and will need to be corrected (Shackel et al., 1992), to account for (i) contributing wood cross-sectional area and (ii) sap flux density heterogeneity (Sperling et al., 2012; Guyot et al., 2015). Other methods use prediction of ET_a spatial variability from related state variables, such as canopy temperature by remote sensing (Nagler et al., 2003), tree stem water potential (Duursma et al., 2008), changes in soil water storage (Sinclair et al., 2005), or from incoming solar radiation and vapor pressure deficit (Gharun et al., 2015). If both ET_a and related variables are available, statistical models such as artificial neural networks (ANN's) can be applied to determine quantitative functions that relate ET_a to a variable number of input variables. ANN's (Gurney, 1997) are being used in

Abbreviations: WS, water storage; MSWP, midday stem water potential; ET_c, potential evapotranspiration rate; C_{rel}, tree relative canopy cover; ET_a, actual evapotranspiration rate; ET_{rel}, relative evapotranspiration; RMSE, root mean square error; SD, standard deviation; DOY, day of year.

* Corresponding author.
E-mail address: vcouvreur@ucdavis.edu (V. Couvreur).

http://dx.doi.org/10.1016/j.agrformet.2016.02.008
0168-1923/

many contexts, ranging from the prediction of soil hydraulic properties using textural information (Tamari et al., 1996; Minasny et al., 2004) to the recognition of handwritten characters (Pal and Singh, 2010).

In this study, we propose to use ANN's in a novel context toward characterization of a field-average relation between potential evapotranspiration rate (ET_c), soil water storage (WS), midday stem water potential (MSWP) and actual evapotranspiration rate (ET_a) in an almond orchard. Subsequently, this relationship is downscaled to the individual tree scale level allowing estimation of spatially-distributed tree-scale ET_a. Finally, the quantitative information is used to analyze local variations in ET_a related to soil and tree water status variability across the orchard.

2. Materials and methods

2.1. Field measurements

Forty trees were monitored in an almond orchard (*Prunus dulcis*) near Lost Hills in Kern County, California, U.S.A. (N35°51′, W119°67′), over a period of 4 years (2009–2012). The almond trees were planted in 1999 on a Milham sandy loam, 6.4 m apart in the direction of the rows, and distant of 7.3 m in the perpendicular direction. The 44 ha orchard (550 m by 800 m) was divided into two blocks respectively watered with drip and fanjet micro-irrigation systems. Each of the two irrigation treatments included 20 monitored trees. The top one meter of soil profile in both blocks was coarse, from sandy clay loam in the fanjet block to sandy loam in the drip block, allowing quick infiltration of irrigation water. Some spatial variations in soil layering and textural properties were reported, though two 20 cm thick fine-textured soil layers were repeatedly observed throughout the blocks, at approximate depths of respectively 130 and 200 cm in the fanjet block, and 130 and 180 cm in the drip block (see Kandelous et al. (2014) and Muhammad et al. (2015) for more details). In order to estimate the root-zone soil water retention curves with the program NeuroMultiStep (Minasny et al., 2004), soil texture and bulk density were measured from undisturbed soil samples collected at 30 cm intervals down to 150 cm for each tree.

Water status was generally measured a day before each irrigation event. Tree water status was measured on lower canopy bagged leaves using a pressure chamber (Pressure Chamber Instrument Model 600) equipped with a portable tank, assuming the measured leaves to be at hydrostatic equilibrium with the tree stem water potential, measured in units of MPa. Though destructive, the pressure bomb method is considered to be an excellent reference measurement for tree water status (Shackel, 2011). For the 4-year period, MSWP was measured for all 40 trees for a total of 75 times, during the growing season starting at the end of March (full leaf set) to early September (harvest). Results are displayed in Fig. 1b, along with the soil WS data.

Soil water content was measured with a neutron probe (Campbell Pacific Nuclear Hydroprobe 503 DR) at 30 cm intervals from 30 to 150 cm depth near the trunk of each of the 40 trees. The neutron probe is considered to be a preferred method for estimation of field-representative soil water storage as it provides an integrative measure of soil water content with a measurement volume corresponding to a radius of about 30 cm. Hence, water content measurements are not as much affected by local soil heterogeneities as TDR's or Echo sensors (Evett et al., 2006). For the 4-year monitoring period, 3000 soil water storage profile evaluations (over 1.5 m soil depth) were carried out (40 locations and 75 measurement times). Soil water storage (cm) data are presented in Fig. 1b, for each of the 4 years, using the day of year (DOY) as the time scale.

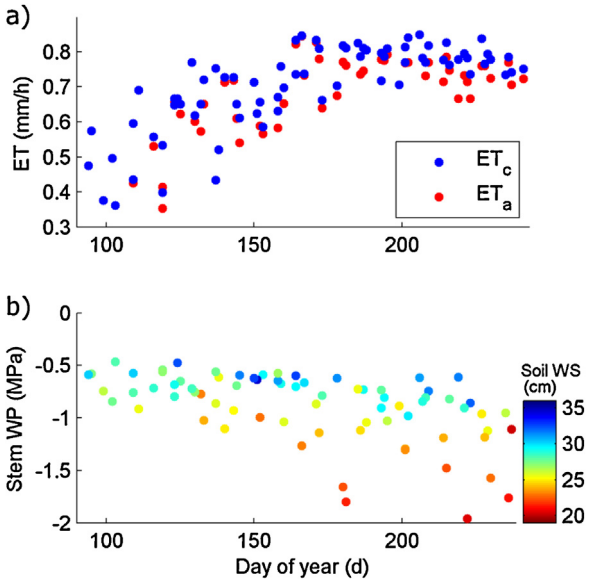

Fig. 1. Field data of (a) weather station ET_c and eddy covariance ET_a, and (b) midday stem water potential (WP) and soil water storage (WS) averaged from 40 tree measurements. The color scale in (a) corresponds to the soil water storage integrated over the root zone (0–1.5 m depth). Data from years 2009 to 2012 are displayed by day of year in this figure.

Field hourly ET_a (mm/h) was measured with a 9 m high triangle type eddy covariance tower located at the center of the orchard (several hundred meters away from the limits of the orchard in all directions). It was equipped at the top with a net radiometer, sonic anemometer, and thermocouples oriented to have no obstructions in the primary upwind direction. For additional details on relevant assumptions and data processing, we refer to Shapland et al. (2013). Midday values were selected in order to correspond to the measurement time of other data. Hourly reference evapotranspiration (ET_0) was obtained from a weather station located approximately 2 km away (Belridge, CIMIS # 146), with tree ET_c (mm/h) computed from multiplication with the almond crop coefficient (K_c). To obtain the K_c values, we assumed that the ET_a/ET_0 ratio corresponds to the ET_c/ET_0 ratio (i.e. K_c) at times the orchard was not water limited (MSWP > −1 MPa). These K_c values displayed a linearly increasing trend over the months covered by the dataset (1.0–1.2 from April to September), which was used to interpolate other K_c values. Nevertheless, ET_a was larger than ET_c for a few days possibly due to the spatial variability of ET_0 or measurement error. In order not to train the ANN to predict ET_a higher than ET_c, we set ET_c equal to ET_a for those few data points, hence at these times the trees are not water stressed.

All data of ET, MSWP and soil WS are presented in Fig. 1, for each of the 4 years, using DOY as the time scale. All presented values are field-average values, simply by computing arithmetic averages from the local scale measurements of the 40 almond trees.

Canopy photo-synthetically active radiation (PAR) interception percentage, or simply referred to as canopy cover was evaluated within one hour of solar noon, once a year during each summer, using a mobile platform lightbar (Lampinen et al., 2012). Unlike yield (Zarate-Valdez et al., 2015; Sanden et al., 2014), canopy cover data can be used to estimate the proportional contribution of individual trees to the field-average ET_c (Goodwin et al., 2005). This information was used when applying local scale ANN to estimate ET_c at the tree scale (see Section 2.3). As trees with higher canopy cover percentage contribute proportionally more to the field-scale ET_c, the latter has to be multiplied by the tree relative canopy cover (C_{rel}, Eq. (1)) to obtain tree ET_c. Thus, in doing so, we assume that tree ET_c is directly proportional to canopy light interception. We

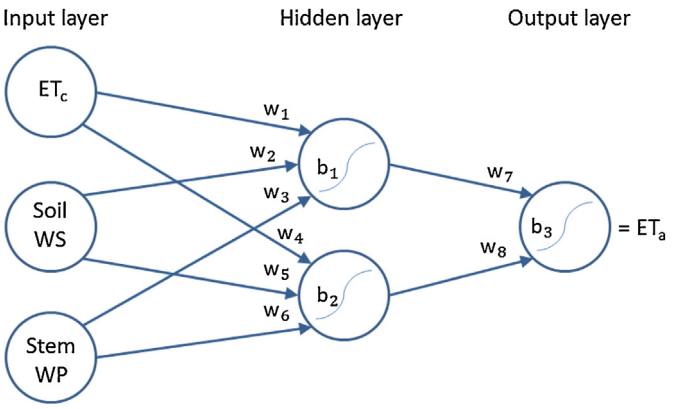

Fig. 2. Scheme of a simple artificial neural network (ANN) with 3 inputs (ET_c, WS and WP), 1 output (actual evapotranspiration), and a single hidden layer composed of 2 neurons. The weights "w" of the neural connections and biases "b" of neurons constitute the trained parameters (numbered as consecutive parameters for simplicity).

pose that the local variations in tree ET_c, using the canopy cover correction will have a direct impact on tree WP as the water potential differential between the average root surface and tree stem xylem increases proportionally to tree evapotranspiration (Landsberg and Fowkes, 1978; Couvreur et al., 2012). Hence, we compute C_{rel} from:

$$C_{rel,i} = \frac{fPAR_i}{\frac{1}{40}\sum_{j=1}^{40} fPAR_j} \quad (1)$$

where $fPAR_i$ is the fraction of intercepted PAR (%) of the ith tree, and j = 1–40 represents the monitored tree number in the summation.

2.2. Artificial neural network approach at the field-scale

The ANN can be represented as a system of neurons organized in three layers (input layer, hidden layer(s), and output layer), as schematically represented in Fig. 2. Each neuron has forward connections with all neurons of the consecutive layer. The signal sent through each connection is amplified or reduced by a weight factor "w". Each neuron of the consecutive layer receives an aggregated signal that serves as an input to a function (here a sigmoid curve with a bias parameter "b") determining the neuron's outgoing signal "a". During a training phase, the weights of neuron connections and the biases of neurons are optimized to fit known "target outputs". For each neuron of the hidden and output layers, the following equation is used to calculate the neuron's outgoing signal "a_{out}" from the incoming signals "a_{in}", associated weights "w_{in}" and bias "b":

$$a_{out} = \left(1 + \exp\left(-b - \sum_{\text{incoming}} w_{in} \cdot a_{in}\right)\right)^{-1} \quad (2)$$

where "*exp*" is the exponential function.

The ANN is applied to determine the relationship between field-scale ET_a (target output) and input variables, represented by 75 observation times of ET_c and 3000 observations of soil WS and tree MSWP (75 times × 40 locations). We used the MATLAB Neural Network toolbox randomly selecting 60% of the field-average data for ANN training and the remaining 40% for validation purposes (default partitioning in the program). As the number of parameters in the ANN strongly increases with the number of neurons "n" in the hidden layer ($5n+1$ rule), it was decided to evaluate the ANN approach using a maximum of 4 neurons in the hidden layer to avoid over-parametrization (note that adding extra input variables would also increase the number of parameters). We discuss later that using more neurons would likely not improve the performance of the ANN.

To evaluate the optimum number of hidden neurons, and to minimize non-uniqueness and local minima issues, we conducted an optimization stage, running 1000 ANN optimizations for each of 1–4 hidden neurons, using independent initial parameter guesses and compositions of the training dataset. As the average prediction of several ANNs can be more accurate than the prediction of any individual ANN (Perrone and Cooper, 1993), a bagging method was used to minimize the root mean squared error (RMSE) of the average predictions (Breiman, 1996) of the best ANNs as follows:

$$\hat{ET}_{a,bag} = \frac{1}{B}\sum_{i=1}^{B} \hat{ET}_{a,i} \quad (3)$$

where $\hat{ET}_{a,bag}$ is the bagged estimator of ET_a, $\hat{ET}_{a,i}$ is the ith best ANN estimator of ET_a using ET_c, MSWP and soil WS as input variables, and B is the total number of best ANN's selected for the bagging method (the value of B is set to minimize the RMSE of the bagged estimator, see Section 3.1);

$$RMSE = \sqrt{\frac{1}{N}\sum_{j=1}^{N}\left(\hat{ET}_{a,bag,j} - ET_{a,meas,j}\right)^2} \quad (4)$$

where $ET_{a,meas,j}$ is the jth measurement of ET_a and N is the total number of ET_a measurements.

Assuming that the 40 monitored trees provide a fair estimation of the field average water status, the ANN seeks for an accurate relation between the field average soil water storage, average midday stem water potential, potential and actual evapotranspiration rates. Hence, the ANN prediction develops a functional relationship that explains field-scale transpiration rate adjustment to soil water limitation using 3 field-averaged state variables. Note that soil surface evaporation is assumed not to be a significant part of ET_a in this study, mainly because of the large canopy cover (83% on average) and relatively dry soil surface (the sandy loam soil favors the quick infiltration of water and the fraction of non-irrigated area between tree rows is about 50% in the fanjet block). Hence canopy transpiration rate and ET_a are considered equivalent.

2.3. Tree-scale ANN prediction

Assuming that individual trees respond to their individual soil WS, MSWP and ET_c couples as they do at the field-average scale, the ANN parametrized for the average field was applied at the tree scale. While tree scale ET_c were estimated by adjusting field ET_c by C_{rel} factors (Section 2.1), soil WS and MSWP were directly measured at the tree scale. They constitute the three input variables required for the ANN to estimate tree scale ET_a.

Field and tree scale frequency distributions of the 3 input types are compared in Fig. 3. We note ranges of local scale variables are close to those averaged at the field scale, whereas frequency distributions between field and tree scale are quite similar. This result warrants the application of the field-average ANN parameters to be applied to the tree scale. According to the classification of Bierkens et al. (2000), this case of downscaling corresponds to a "deterministic relation with auxiliary information available", where the average value of the predicted variable (ET_a) is known at large scale.

3. Results and discussion

3.1. Artificial neural network approach at the field scale

The ANN approach at the field scale allowed for training relations between ET_c, soil WS, MSWP and ET_a. The networks with

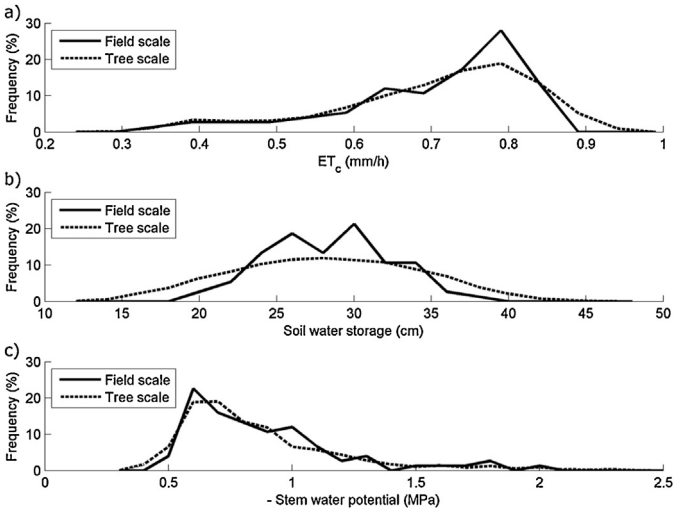

Fig. 3. ANN input frequency distributions (%) for (a) ET_c, (b) soil WS and (c) MSWP, at field scale (solid lines) and tree scale (dashed lines). Field scale distributions use 75 realizations while tree scale distributions use 3000 data sets (75 times × 40 trees). Both are reported as frequency percentage.

2 neurons in the hidden layer (Fig. 2) were more optimal in the sense that they had (i) the lowest median RMSE in the validation phase (evaluated from the corresponding 1000 ANNs), (ii) the lowest individual RMSE in the validation phase, and (iii) the lowest individual RMSE aggregating both training and validation phases. Counter-intuitively, our analysis showed that increasing the number of neurons in the hidden layer above two increased the validation RMSE value. Seemingly, the additional neurons and complexity tended to generate an over-fitting of the training data set that added additional noise in the validation set. This suggests that given the simplicity of this ANN problem (i.e., one output, three input types and likely presence of some noise in measurements), a solution of relatively low complexity is more appropriate.

Fig. 4a compares the eddy covariance observations of field ET_a with ANN predictions using the bagging method. The RMSE was minimized when bagging predictions from the 4 best ANNs ($B = 4$ in Eq. (3)). Its value went down to 0.0246 mm/h with an R^2 of 0.944 for the combined training and validation data. Both higher and lower values of B increased the RMSE of the bagged estimator of ET_a.

3.2. Artificial neural network approach at the tree scale

Applying the ANN optimized in Section 2.1 to individual trees' ET_c, soil WS and MSWP allowed for prediction of tree scale ET_a. In Fig. 4(b), we show that a major driver of tree-scale ET_a variability is the tree relative canopy cover (C_{rel}) represented by the color scale. Specifically, tree-scale ET_a can be reduced by about 50% relative to field ET_a, in one instance due to very low C_{rel} values (orange and dark red points). These points represent a single tree for two consecutive years. For all other trees, tree-scale ET_a seldom exceeds 15% relative difference from field average, as controlled by variations in C_{rel}.

Two other sources of variability of tree ET_a (soil WS and tree MSWP) are presented in Fig. 5 for a field-representative sample of 20 individual trees (10 each for fanjet and drip irrigation blocks), during the growing season for all 4 years. To better illustrate water stress effects on tree ET, we plotted actual ET_a, relative to potential tree ET (ET_c), or ET_{rel}. Hence, for conditions of no water stress, this ratio should be around 1.0.

As one would expect, the ANN-predicted ET_{rel} decreases with a reduction in soil WS (as presented by the fitted curves in Fig. 5) and responds drastically to MSWP when it is below −1.5 MPa (see color scale), as also demonstrated by Sinclair et al. (2005) and Shackel (2011). At these low water potential values, the large standard deviation values (vertical lines, representing variation among the 4 ANN predictions) indicate that even though the ANNs predict a clear reduction of the ET_{rel}, there remains a major source of uncertainty on the quantitative response. We note that ANN prediction variation is low at high MSWP values (closer to zero), indicating that the control of MSWP is low for non-stressed conditions as well as a robust prediction that is relatively unique.

Even though the same bagged ANNs are used for all monitored trees, the variation of control of MSWP and soil WS on ET_{rel} among the 40 monitored trees was large. Specifically, most of the drip irrigated trees (bottom panel in Fig. 5) did not show marked signs of water stress at low soil WS levels, as evidenced by relatively higher MSWP and ET_{rel} values closer to 1.0. One could provide many explanations for this differentiation in soil WS response. Specifically, one may conclude that water stress response varies among irrigation type (Feddes et al., 1978) or is controlled by difference in root distribution affecting access to soil available water and root hydraulic conductance (Couvreur et al., 2014b). Others may argue that differential tree response is determined by soil WS measurement uncertainty due soil moisture heterogeneity (Andreu et al., 1997; Beff et al., 2013; Warrick and Lazarovitch, 2007).

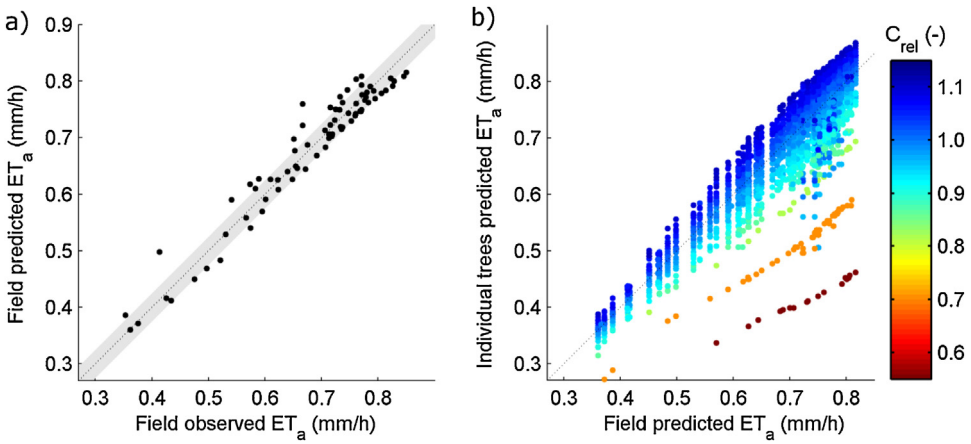

Fig. 4. (a) Field observed ET_a (eddy covariance tower) versus neural network bagged prediction of ET_a at the field scale. The straight line represents the 1:1 relation and the gray region defines the range of ±1 standard deviation (0.0246 mm/h). (b) Comparison of field with individual trees ET_a predicted by the bagged best neural networks. The color scale indicates the tree relative canopy cover (C_{rel}) of individual trees as compared to the average field.

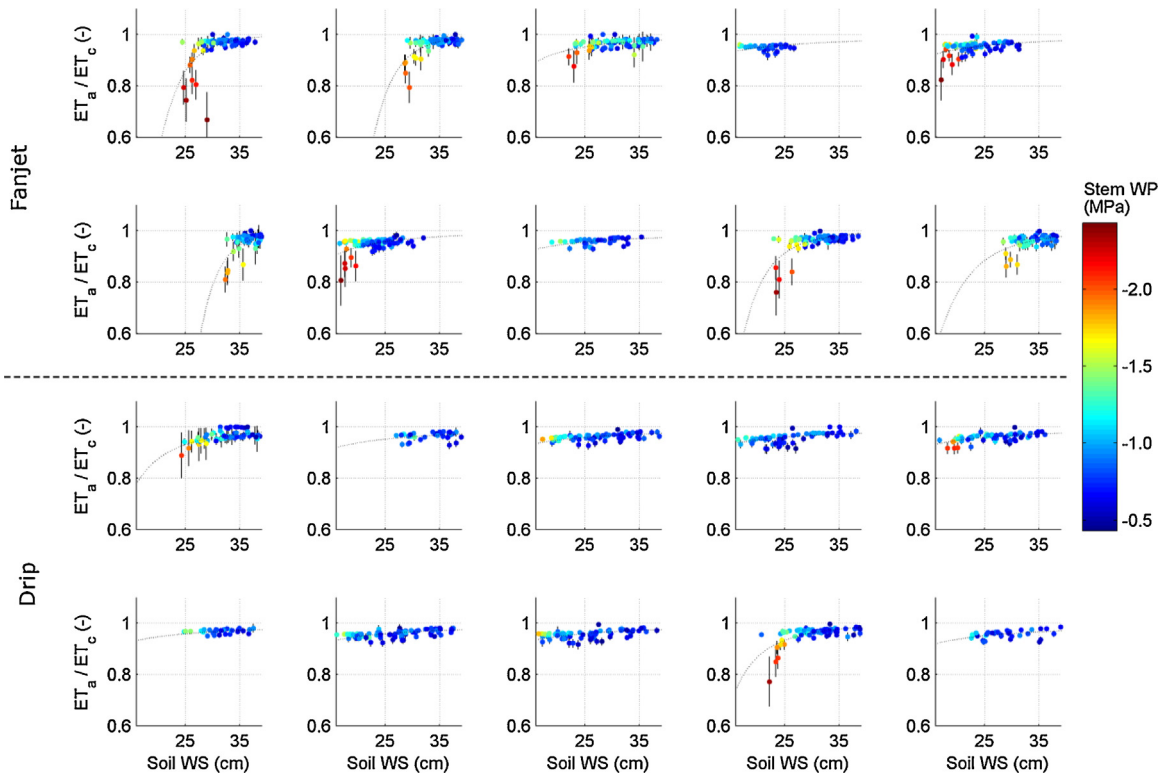

Fig. 5. Tree-scale relative transpiration reduction factor versus soil water storage in the top 1.5 m predicted by bagging of the best neural networks for 20 irrigated trees. The color scale indicates individual trees midday stem water potential. Vertical bars indicate the standard deviations of predictions by the ANNs included in the bagging. The trend is represented with the fitted curve.

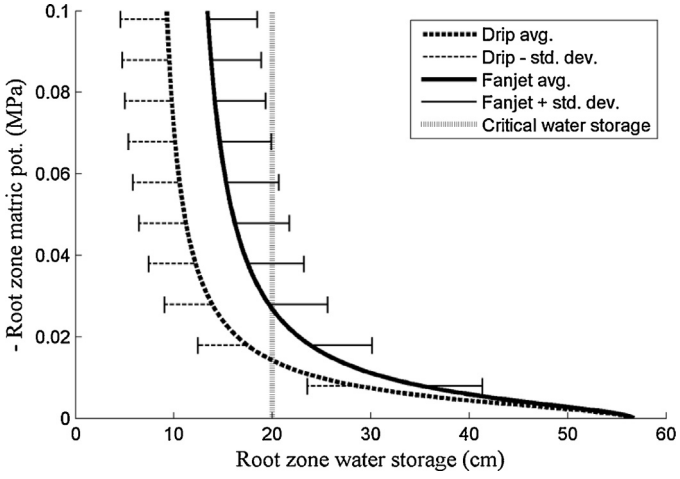

Fig. 6. Average root-zone water storage (cm) and associated matric potentials predicted by *NeuroMultistep* with corresponding standard deviation values (error bars) in drip (dotted lines) and fanjet (solid black lines) irrigated blocks. The critical soil water storage beyond which water stress frequently occurs in the fanjet block (20 cm) is marked by the vertical gray line.

In this specific case, we analyzed the effect of soil textural differences between the two irrigated blocks and the resulting effect on root zone water potential. For this purpose, average soil water retention curves for the rooting zone of the fanjet and drip irrigated blocks were estimated from the 40 tree locations using soil texture and bulk soil density values as input to the program *NeuroMultiStep* (Minasny et al., 2004). The corresponding block-average soil water retention curves for a range of matric potentials between 0 and −0.1 MPa are presented in Fig. 6, together with block variation represented by horizontal bars of magnitude equal to corresponding standard deviations of soil water storage (WS, cm) to the 1.5 m rooting zone depth. Although the root zone of the drip-irrigated block is of a slightly coarser soil texture (thus expected to hold less water and show more water stress), it received more irrigation water on average (4% more over the 4 years) and was less subject to drying by soil surface evaporation, which allowed maintenance of a similar soil WS in both blocks. As Fig. 6 shows, the average root zone soil water retention curve for the drip-irrigated block lies below that of the fanjet block. Hence for any given soil WS, the average root zone water potential, which can be assimilated to a plant-sensed soil water potential (Couvreur et al., 2014a), is more negative for the fanjet block. Differences in root zone water potential between blocks become particularly large at a critical soil WS of 20 cm (corresponding to a root zone volumetric water content of 0.13 cm^3 cm^{-3} for the 1.5 m rooting zone) at which marked differences in ET_{rel} response generally occurred.

In the following, we quantify tree ET_a variability using frequency distributions. The downscaled ET_a followed a normal distribution across the field (see Fig. 7a), as well as for both irrigation treatments (see Fig. 7b and c). During well-watered periods (field average MSWP higher than −1 MPa), the standard deviation (SD) of ET_a is close to 5%, about equal to the C_{rel} variability. When isolating periods of water stress conditions (field average MSWP lower than −1.5 MPa), the SD of ET_a increased to 7.6% for the whole field (Fig. 7a). This value is included in the range observed in almond by Gonzalez-Dugo et al. (2013), who also reports increasing variability in drier conditions (from 7.3 to 10.1% for average stem WP of respectively −1.59 and 3.04 MPa). Interestingly, soil water content variability is also reported to increase in drying conditions (Famiglietti et al., 2008; Vereecken et al., 2008; Beff et al., 2013), but with higher relative standard deviations (more than 20% in similar conditions), which suggests that the field scale variability of tree ET_a response is smoothed out, or shifted, as compared to the variability of soil water content at the same scale.

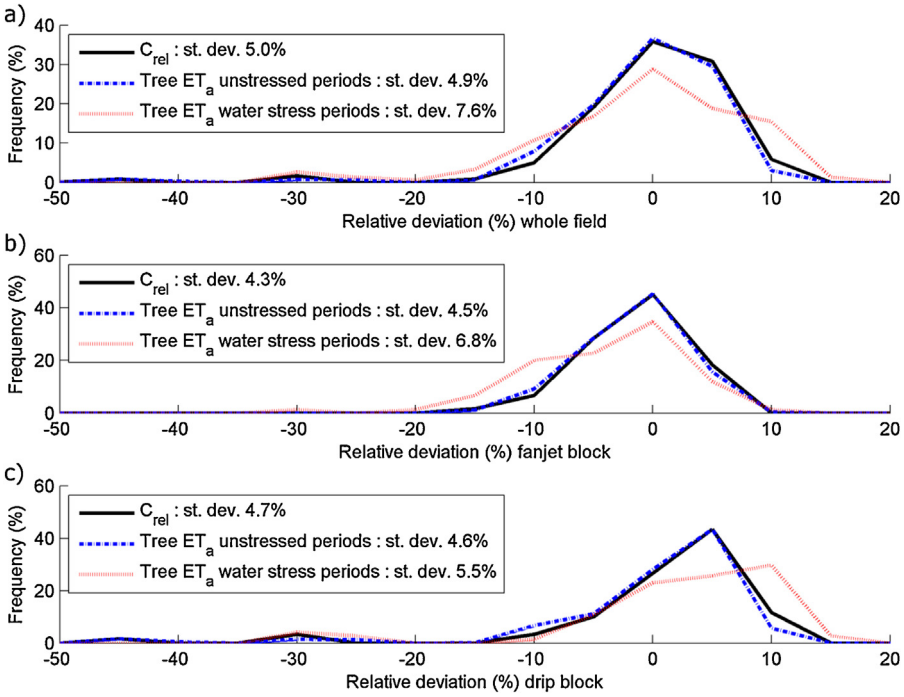

Fig. 7. Frequency distributions of tree relative canopy cover (C_{rel}, black solid lines), tree ET_a for field-average MSWP values larger than −1 MPa (light blue lines), and tree ET_a for field-average MSWP lower than −1.5 MPa (red lines) for (a) whole field, (b) fanjet block and (c) drip irrigated block.

Standard deviation values were smaller for the individual irrigation blocks, implying that a significant source of ET_a variability is caused by block differences in water stress response, as explained by different soil water retention functions between blocks (Fig. 6). Under well-watered conditions, values of ET_a in the drip block were 1.7% higher than the field-average. This difference increased to 4.4% when considering water stress periods only.

The assumption that the field scale ANN is applicable to the tree scale must be considered carefully, though it constitutes our best guess in the ET_a downscaling problem. Quantitatively, the predicted tree scale ET_a correction is well supported by independent results using the water balance method for the same experimental field (Kandelous et al., 2014) that need to be corrected for tree ET_a in the fanjet block not to predict unlikely amounts of capillary rise at long term. For instance, using our presented approach, the tree that is closely monitored in the fanjet block in Kandelous et al. (2014) is predicted to transpire 5.4% less than the field average, thereby fully eliminating the unlikely capillary rise (34.2 ± 4.7 cm) that was estimated using the water balance approach.

4. Conclusion

This study used an artificial neural network (ANN) approach to downscale field ET to the individual tree scale. Assuming that individual trees respond to combinations of their MSWP, soil WS and ET_c in the same way as the average field would, the field scale optimized ANN was used to downscale ET_a to the tree level. Our analysis determined that tree ET and response to water stress could be assessed using a combined dataset of MSWP, soil WS and ET_c. We concluded that relative canopy cover (C_{rel}) was the main source of variability of actual tree ET, ET_a, while MSWP was the most controlling factor for ET_{rel}. We also concluded that tree response to soil water stress was largely controlled by effective root zone soil properties. Specifically, our analysis showed that tree response to soil water stress was different between the fanjet and drip-irrigated blocks because of soil textural differences and associated soil water retention properties. The predicted tree ET_a followed a normal distribution (with standard deviation of about 5%), which was close to the C_{rel} distribution for non-stressed soil conditions. However, standard deviation values increased (7.6% for the whole orchard) when considering periods for water stress conditions only.

Acknowledgements

We acknowledge funding by the Almond Board of California, through project “Fertigation: interaction of water and nutrient management in almonds – monitoring water use (ET), stress & yield impacts” (12.HORT11A), with Dr. Patrick Brown as its principal investigator.

We warmly thank Dr. Richard L. Snyder for his help in analyzing the energy balance data.

During the preparation of this manuscript, V.C. was supported by the “Belgian American Educational Foundation” (BAEF) as UCLouvain Fellow, by “Wallonie-Bruxelles International” (WBI) with a WBI.WORLD excellence grant, and by the “Fonds Spéciaux de Recherche” (FSR) of the Université catholique de Louvain.

References

Andreu, L., Hopmans, J.W., Schwankl, L.J., 1997. Spatial and temporal distribution of soil water balance for a drip-irrigated almond tree. Agric. Water Manage. 35, 123–146, http://dx.doi.org/10.1016/s0378-3774(97)00018-8.

Beff, L., Günther, T., Vandoorne, B., Couvreur, V., Javaux, M., 2013. Three-dimensional monitoring of soil water content in a maize field using Electrical Resistivity Tomography. Hydrol. Earth Syst. Sci. 17, 595–609.

Bierkens, M.F.P., Finke, P.A., De Willigen, P., 2000. Upscaling and Downscaling Methods for Environmental Research, Developments in Plant and Soil Sciences. Springer, 204 pp.

Breiman, L., 1996. Bagging predictors. Mach. Learn. 24, 123–140.

Couto, A., Padin, A.R., Reinoso, B., 2013. Comparative yield and water use efficiency of two maize hybrids differing in maturity under solid set sprinkler and two different lateral spacing drip irrigation systems in Leon, Spain. Agric. Water Manage. 124, 77–84.

Couvreur, V., Vanderborght, J., Javaux, M., 2012. A simple three-dimensional macroscopic root water uptake model based on the hydraulic architecture approach. Hydrol. Earth Syst. Sci. 16, 2957–2971.

Couvreur, V., Vanderborght, J., Beff, L., Javaux, M., 2014a. Horizontal soil water potential heterogeneity: simplifying approaches for crop water dynamics models. Hydrol. Earth Syst. Sci. 18, 1723–1743.
Couvreur, V., Vanderborght, J., Draye, X., Javaux, M., 2014b. Dynamic aspects of soil water availability for isohydric plants: focus on root hydraulic resistances. Water Resour. Res. 50, 8891–8906.
Dabach, S., Lazarovitch, N., Šimůnek, J., Shani, U., 2013. Numerical investigation of irrigation scheduling based on soil water status. Irrigation Sci. 31, 27–36.
Dabach, S., Shani, U., Lazarovitch, N., 2015. Optimal tensiometer placement for high-frequency subsurface drip irrigation management in heterogeneous soils. Agric. Water Manage. 152, 91–98.
Duursma, R.A., Kolari, P., Perämäki, M., Nikinmaa, E., Hari, P., Delzon, S., Loustau, D., Ilvesniemi, H., Pumpanen, J., Mäkelä, A., 2008. Predicting the decline in daily maximum transpiration rate of two pine stands during drought based on constant minimum leaf water potential and plant hydraulic conductance. Tree Physiol. 28, 265–276.
Eching, S.O., Hopmans, J.W., Wallender, W.W., 1994. Estimation of in situ unsaturated soil hydraulic functions from scaled cumulative drainage data. Water Resour. Res. 30, 2387–2394.
Evett, S.R., Tolk, J.A., Howell, T.A., 2006. Soil profile water content determination: sensor accuracy, axial response, calibration, temperature dependence, and precision. Vadose Zone J. 5, 894–907.
Famiglietti, J.S., Ryu, D., Berg, A.A., Rodell, M., Jackson, T.J., 2008. Field observations of soil moisture variability across scales. Water Resour. Res. 44, http://dx.doi.org/10.1029/2006wr005804.
Feddes, R.A., Kowalik, P.J., Zaradny, H., 1978. Simulation of Field Water Use and Crop Yield. Pudoc, 189 pp.
Fischer, G., van Velthuizen, A., Nachtergaele, F.O., 2000. Global agro-ecological zones assessment: methodology and results. Interim Report. International Institute for Applied Systems Analysis, Laxenburg, Austria.
Gharun, M., Turnbull, T.L., Henry, J., Adams, M.A., 2015. Mapping spatial and temporal variation in tree water use with an elevation model and gridded temperature data. Agric. Forest Meteorol. 200, 249–257.
Gonzalez-Dugo, V., Zarco-Tejada, P., Nicolás, E., Nortes, P.A., Alarcón, J.J., Intrigliolo, D.S., Fereres, E., 2013. Using high resolution UAV thermal imagery to assess the variability in the water status of five fruit tree species within a commercial orchard. Precis. Agric. 14, 660–678.
Goodwin, I., Whitfield, D.M., Connor, D.J., 2005. Effects of tree size on water use of peach (*Prunus persica* L. Batsch). Irrig. Sci. 24, 59–68.
Gurney, K., 1997. An Introduction to Neural Networks. Routledge, London, 135 pp.
Guyot, A., Ostergaard, K.T., Fan, J.L., Santini, N.S., Lockington, D.A., 2015. Xylem hydraulic properties in subtropical coniferous trees influence radial patterns of sap flow: implications for whole tree transpiration estimates using sap flow sensors. Trees-Struct. Funct. 29, 961–972.
Hopmans, J.W., Schoups, G.H., 2005. Soil water flow at different spatial scales. In: Anderson, G. (Ed.), Encyclopedia of Hydrological Sciences. Wiley, Chichester, UK, pp. 999–1010.
IPCC, 2012. Summary for Policymakers, Managing the Risks of Extreme Events and Disasters to Advance Climate Change Adaptation. A Special Report of Working Groups I and II of the Intergovernmental Panel on Climate Change.
Kandelous, M.M., Kamai, T., Vrugt, J.A., Simunek, J., Hanson, B., Hopmans, J.W., 2012. Evaluation of subsurface drip irrigation design and management parameters for alfalfa. Agric. Water Manage. 109, 81–93.
Kandelous, M.M., Brown, P.H., Sanden, B.L., Hopmans, J.W.,2014. Optimization of water and nitrate use efficiencies for almonds under micro-irrigation. In: 2013–2014 Annual Research Report. Almond Board of California, 26 pp, http://www.almondboard.com/PR/A.2013.13-PREC4-Hopmans.Hopmans.Optimization%20of%20Water%20and%20Nitrate%20Use%20Efficiencies%20Under%20Micro-Irrigation.pdf.
Lampinen, B.D., Udompetaikul, V., Browne, G.T., Metcalf, S.G., Stewart, W.L., Contador, L., Negrón, C., Upadhyaya, S.K., 2012. A mobile platform for measuring canopy photosynthetically active radiation interception in orchard systems. HortTechnology 22, 237–244.
Landsberg, J.J., Fowkes, N.D., 1978. Water-movement through plant roots. Ann. Bot. -London 42, 493–508.
Minasny, B., Hopmans, J.W., Harter, T., Eching, S.O., Tuli, A., Denton, M.A., 2004. Neural networks prediction of soil hydraulic functions for alluvial soils using multistep outflow data. Soil Sci. Soc. Am. J. 68, 417–429.
Muhammad, S., Sanden, B.L., Lampinen, B.D., Saa, S., Siddiqui, M.I., Smart, D.R., Olivos, A., Shackel, K.A., DeJong, T., Brown, P.H., 2015. Seasonal changes in nutrient content and concentrations in a mature deciduous tree species: Studies in almond (*Prunus dulcis* (Mill.) D. A. Webb). Eur. J. Agron. 65, 52–68.
Nagler, P.L., Glenn, E.P., Lewis Thompson, T., 2003. Comparison of transpiration rates among saltcedar, cottonwood and willow trees by sap flow and canopy temperature methods. Agric. Forest Meteorol. 116, 73–89.
Pal, A., Singh, D., 2010. Handwritten English character recognition using neural network. Int. J. Comput. Sci. Commun. 1, 141–144.
Parry, M.L., et al., 2007. Climate Change 2007: Impacts, Adaptation and Vulnerability. Contribution of Working Group II to the Fourth Assessment Report of the Intergovernmental Panel on Climate Change. Cambridge Univ. Press.
Perrone, M.P., Cooper, L.N., 1993. When networks disagree: ensemble methods for hybrid neural networks. In: Mammone, R.J. (Ed.), Neural Networks for Speech and Image Processing. Chapman-Hall, New York.
Sanden, B.L., Muhammad, S., Brown, P.H., Brown, K.A., Snyder, R.L., 2014. Correlation of individual tree nut yield, evapotranspiration, tree stem water potential, total soil salinity and chloride in a high production almond orchard. J. Am. Soc. Agric. Biol. Eng. 6, 4337–4344.
Shackel, K., 2011. A plant-based approach to deficit irrigation in trees and vines. Hortscience 46, 173–177.
Shackel, K.A., Johnson, R.S., Medawar, C.K., Phene, C.J., 1992. Substantial errors in estimates of sap flow using the heat-balance technique on woody stems under field conditions. J. Am. Soc. Hortic. Sci. 117, 351–356.
Shapland, T.M., McElrone, A.J., Paw, U.K.T., Snyder, R.L., 2013. A turnkey data logger program for field-scale energy flux density measurements using eddy covariance and surface renewal. Italian J. Agrometeorol. 1, 1–9.
Shi, J., Li, S., Zuo, Q., Ben-Gal, A., 2015. An index for plant water deficit based on root-weighted soil water content. J. Hydrol. 522, 285–294.
Sinclair, T.R., Holbrook, N.M., Zwieniecki, M.A., 2005. Daily transpiration rates of woody species on drying soil. Tree Physiol. 25, 1469–1472.
Sperling, O., Shapira, O., Cohen, S., Tripler, E., Schwartz, A., Lazarovitch, N., 2012. Estimating sap flux densities in date palm trees using the heat dissipation method and weighing lysimeters. Tree Physiol. 32, 1171–1178.
Stanhill, G., 1986. Water use efficiency. In: Brady, N.C. (Ed.), Advances in Agronomy. Academic Press, pp. 53–85.
Tamari, S., Wösten, J.H.M., Ruiz-Suárez, J.C., 1996. Testing an artificial neural network for predicting soil hydraulic conductivity. Soil Sci. Soc. Am. J. 60, 1732–1741.
Tanji, K.K., Kielen, N.C., 2002. Agricultural Drainage Water Management in Arid and Semi-Arid Areas, FAO Irrigation and Drainage Paper 61. FAO, Rome.
Vereecken, H., Kamai, T., Harter, T., Kasteel, R., Hopmans, J.W., Huisman, J.A., Vanderborght, J., 2008. Comment on "Field observations of soil moisture variability across scales". Water Resour. Res. 44, W12601, http://dx.doi.org/10.1029/2008WR006911.
Warrick, A.W., Lazarovitch, N., 2007. Infiltration from a strip source. Water Resour. Res. 43 (5), http://dx.doi.org/10.1029/2006wr004975.
Zarate-Valdez, J.L., Muhammad, S., Saa, S., Lampinen, B.D., Brown, P.H., 2015. Light interception, leaf nitrogen and yield prediction in almonds: a case study. Eur. J. Agron. 66, 1–7.